Applied Research Laboratory

Technical Report

Acoustic Intensity in the Interaction Region of a Parametric Sonar

PENNSTATE

The Pennsylvania State University
APPLIED RESEARCH LABORATORY
P.O. Box 30
State College, PA 16804

Acoustic Intensity in the Interaction Region of a Parametric Sonar

by

Thomas B. Gabrielson
Gerald C. Lauchle
James A. McConnell
David J. Van Tol
Nelson F. Kottke

Technical Report 02-017
December 2002

Supported by:
Office of Naval Research

REPORT DOCUMENTATION PAGE

Form Approved
OMB No. 0704-0188

1. REPORT DATE (DD-MM-YYYY)	2. REPORT TYPE	3. DATES COVERED (From - To)
December 2002	Technical Report	

4. TITLE AND SUBTITLE

Acoustic Intensity in the Interaction Region of a Parametric Sonar

5a. CONTRACT NUMBER
BOA N00014-00-G-0058/0024

5b. GRANT NUMBER

5c. PROGRAM ELEMENT NUMBER

5d. PROJECT NUMBER

5e. TASK NUMBER

5f. WORK UNIT NUMBER

6. AUTHOR(S)

Thomas B. Gabrielson, Gerald C. Lauchle, James A. McConnell, David J. Van Tol and Nelson F. Kottke

7. PERFORMING ORGANIZATION NAME(S) AND ADDRESS(ES)

Applied Research Laboratory
The Pennsylvania State University
P. O. Box 30
State College, PA 16804-0030

8. PERFORMING ORGANIZATION REPORT NUMBER

9. SPONSORING / MONITORING AGENCY NAME(S) AND ADDRESS(ES)

Office of Naval Research
800 North Quincy Street
Arlington, VA 22217

10. SPONSOR/MONITOR'S ACRONYM(S)

11. SPONSOR/MONITOR'S REPORT NUMBER(S)

12. DISTRIBUTION / AVAILABILITY STATEMENT

13. SUPPLEMENTARY NOTES

14. ABSTRACT

The fundamental goal of this project was to measure acoustic intensity in the strong interaction region of a parametric source. The expected benefits of such a measurement are (1) a clear definition of the source-generation region, and (2) an ability to separate local generation (the reactive field) from propagation (the real or active field).

15. SUBJECT TERMS

16. SECURITY CLASSIFICATION OF:			17. LIMITATION OF ABSTRACT	18. NUMBER OF PAGES	19a. NAME OF RESPONSIBLE PERSON
a. REPORT	b. ABSTRACT	c. THIS PAGE			Thomas B. Gabrielson
UNCLASSIFIED	UNCLASSIFIED	UNCLASSIFIED	UNLIMITED	30	19b. TELEPHONE NUMBER (Include area code) (814) 865-1370

TABLE OF CONTENTS

		Page
Table of Contents		ii
List of Figures		iii
Executive Summary		2
Report on Lake Seneca Measurements:		
I.	Introduction	3
II.	Acoustic Intensity	5
III.	Test Configuration	6
IV.	Characteristics of the Projector	8
V.	Influence of Nonlinearity	11
VI.	Errors in the Intensity Probes – Theory	14
VII.	Summary of Measurements	16
VIII.	Errors in the Intensity Probes – Measurement and Calibration	21
IX.	Improvements and Lessons Learned	25
Acknowledgements		27

LIST OF FIGURES

Figure		Page
1.	A schematic illustration of parametric generation.	3
2.	The TOwed Parametric Sonar (TOPS) projector panel on the left has a radiating face 21 inches by 17 inches and produces the primary beams at 22 kHz and 27 kHz simultaneously	7
3.	The two varieties of acoustic intensity sensors used in this experiment.	7
4	The configuration of the sensors and the source.	8
5.	The primary and secondary beam patterns measured using a reference hydrophone 11 meters from the projector	9
6.	The secondary beam pattern from Figure 5 normalized so that its maximum is 0 dB.	10
7.	Spectrum of the synthesized waveform with the sum of the two primary-frequency signals (P_1 and P_2).	11
8.	Spectrum of the voltage monitor signal at the output of the projector power amplifier.	12
9.	A typical received spectrum at 8.5 meters from the projector.	13
10.	Beam patterns (in azimuth) as measured by a reference hydrophone (p_{ref}) and by the four hydrophones (p_{1-4}) that comprise the *p-p* prob.	16
11.	Active (blue) and reactive (red) acoustic intensity as measured by the on-axis component of the *p-a* probe.	17
12.	Active (blue) and reactive (red) acoustic intensity as measured by the cross-axis component of the *p-a* probe.	17
13.	A comparison of the active intensity calculated from both the *p-a* probe and the *p-p* probe.	18
14.	Measured phase difference between hydrophones in the *p-p* probe as a function of azimuth angle.	19

15. Active intensity for both the *p-a* probe and the *p-p* probe. 20

16. The on-axis reactive intensity. 21

17. Results from a rotational interchange calibration at 5 kHz of the on-axis hydrophone pair in the *p-p* probe. 23

18. The interchange calibration at 5 kHz also produces a measure of the relative acoustic field between the two hydrophones. 23

EXECUTIVE SUMMARY

Research Goal

The fundamental goal of this project was to measure acoustic intensity in the strong interaction region of a parametric source. The expected benefits of such a measurement are (1) a clear definition of the source-generation region, and (2) an ability to separate local generation (the reactive field) from propagation (the real or active field).

Results and Interpretation

Acoustic intensity was measured in the parametric interaction region of the TOPS (TOwed Parametric Sonar) projector at Lake Seneca. The TOPS was driven with primary signals at 22 kHz and 27 kHz producing a secondary wave at 5 kHz. In a parametric source, two primary signals are transmitted from a projector. The levels of these primaries are sufficiently high that nonlinearity in the water cannot be neglected. As the primaries propagate, this nonlinearity produces both sum- and difference-frequency components. The difference-frequency component (the secondary wave) is the desired product having a beam width determined not by the physical dimensions of the projector but by the shape of the primary beams and by the length of the region of significant interaction in the water. The source of the secondary is not the projector but it is a region of water in front of the projector.

The receiving sensors were located 8.5 meters from the projector. At that range, the secondary was between 40 and 45 dB below either primary. The intensity measurements were made at fixed range but varying azimuth angle and varying depth thus developing a two-dimensional cross-section of the secondary beam.

Parametric beams have been studied extensively in the past but with pressure measurements only. This experiment is the first measurement of pressure, acoustic particle motion, and acoustic intensity in a parametric beam.

The measurements of active intensity appear to be of good quality and represent the propagating component of the secondary wave with reasonable accuracy. The measurements of reactive intensity (associated with local generation of the secondary) are intriguing but suspect. While there is some indication of a true secondary-wave generation component, there are sufficient ambiguities in the reactive-field measurement that definite conclusions cannot be made without further investigation.

Beyond the acoustic intensity measurements themselves, the principal value in this set of measurements is in the techniques developed and the lessons learned. This exercise has demonstrated the practicality of measuring acoustic intensity in a parametric beam but the investigation has also led to the development of several techniques to ensure high-quality data collection. A deep understanding of the parametric generation mechanism will result in more effective applications of parametric sonar and less effort wasted in ineffective applications.

REPORT ON LAKE SENECA MEASUREMENTS

I. Introduction

Figure 1 shows, schematically, the evolution of the beams in a parametric sonar. The projector (at the left) radiates high-frequency sound (the primary beam) in a conventional manner. The sound level is sufficiently high that nonlinearity in the medium can no longer be neglected. If a single primary frequency is radiated, nonlinear interaction produces a component at twice the primary frequency (and three times and so on) and a component of DC pressure (related to "radiation pressure"). This nonlinear generation is proportional to the square of the primary pressure so, for moderate levels of primary radiation, the nonlinear products can be quite small.

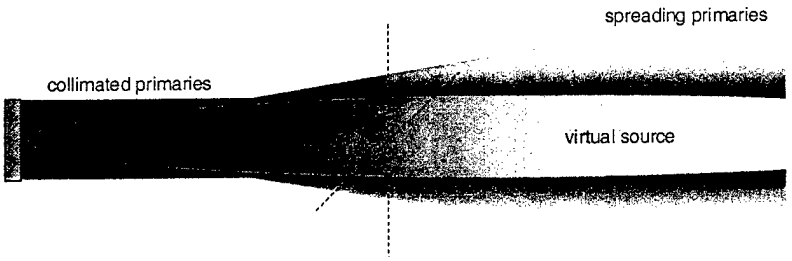

Figure 1. A schematic illustration of parametric generation. A projector (left side) produces a beam consisting of two primary frequency waves (blue). These waves are of sufficiently high amplitude that nonlinearity in the water produces a difference frequency or secondary beam (red). The secondary is produced in the water rather than directly from the projector. The rate of generation depends on the amplitudes, which depend on spreading and absorption losses.

If the primary radiation consists of two frequencies, then the nonlinear interaction results in generation of the sum and difference frequencies in addition to harmonics of the primary frequencies. The difference (or secondary) frequency is generally the desired product in a parametric system. Within limits, the amplitude of the secondary wave can be increased by increasing the amplitude of the primary waves.

However, two processes limit the ultimate level at the primary frequency. At some point, the transducer may cavitate and further increases in drive power are ineffective in increasing the primary pressure level. Also, power is transferred from the primaries not only to the secondary but also to harmonic generation. As the primary power level increases, the rate of generation of higher harmonics increases and this reduces the pressure level at the original frequencies for difference-frequency generation. In the absence of significant absorption or spreading, the primary pressure waves eventually form shock waves as a result of harmonic generation. Once harmonic generation becomes significant, the level of generation of the difference frequency drops rapidly.

Since generation of the difference frequency wave (the "secondary" beam) is proportional to the product of the pressures of the two primary frequency waves, a reduction by a factor of two in the primary amplitudes results in a reduction by a factor of four in the amplitude of the secondary. Furthermore, nonlinearity in water is relatively weak so the process is inefficient at best. Two of the keys to understanding parametric generation are that (1) the nonlinearity is weak and (2) the secondary generation is proportional to the product of the amplitudes of the two primaries.

Beyond nonlinear generation of higher harmonics of the primaries, there are two other mechanisms that cause reduction in primary pressure levels. Spreading of the primary beams produces a decrease in amplitude (in both primary beams) proportional to $1/r$ once geometric spreading becomes important. Also, acoustic absorption reduces the primary-wave pressure amplitude beyond the reductions from spreading.

There are scale distances associated with each of these three effects. For a transducer with dimensions larger than the primary wavelength, there is a near-field ("Fresnel") region in which there is very little geometric spreading and the envelope of the pressure amplitude does not decrease with range. While the transition between the near-field and the far-field regions is not sharp, it can be estimated. One measure is the distance to the furthest interference peak on the beam axis. For a circular piston with radius, a, in a rigid baffle, this distance is given by $r = a^2/\lambda$. At distances shorter than this transition distance, the amplitudes of the primary waves can be considered to be roughly constant. At distances beyond the transition range, the amplitude drops as $1/r$ for each primary (so the generated amplitude of the secondary drops as $1/r^2$).

The scale distance associated with loss of power in the original primary waves to harmonic generation is the shock inception distance. For plane waves (i.e., no spreading), the shock inception distance is

$$R_{shock} = \frac{1}{\beta M k} \qquad (1)$$

where β is the nonlinearity parameter (3.5 for water), M is the acoustic Mach number (acoustic particle speed divided by the sound speed), and k is the wave number. For the primary pressure levels used in this experiment, the acoustic Mach number was no greater than 0.0002. Therefore, the minimum shock inception distance at 24.5 kHz would have been 14 meters. This is well into the region of spherical spreading so neither shocks nor excessive power loss to harmonics would be expected.

The scale distance associated with absorption is the absorption length normally defined as the distance at which the amplitude has dropped by $1/e$ solely from absorption (i.e., over and above spreading). The absorption length at 24.5 kHz is over 65 km in freshwater and more than 3 km in seawater so absorption is negligible for this experiment.

The parametric source used in this project (the TOwed Parametric Sonar – TOPS) produced primary beams in which the near-field length was shorter than the shock inception distance and much smaller than the absorption distance. For this configuration, most of the secondary power is generated within two or three times the collimation length. (The parametric interaction length is often taken to be the absorption length but this is an artifact of the accounting associated with the apparent source level. The *apparent* source level does continue increasing over the absorption length but, as the distance from the projector increases, so does the exaggeration of locally generated levels by translation back to the projector.)

II. Acoustic Intensity

Measurements of acoustic pressure alone cannot distinguish between propagating waves and reactive fields. In many instances, this distinction is not important; however, in the parametric source, the secondary wave is not generated directly by the transducer. The secondary is generated in a volume of the water in the primary beam. At any range in this generation region, there should be two wave components: (1) a propagating component representing secondary power that has already been produced at shorter ranges by nonlinear interaction, and (2) a source-generation component that is related to the local production of secondary power.

Acoustic intensity is a vector quantity so the direction of propagation can be determined. In addition, total intensity has two parts – a real part associated with the propagating power, and an imaginary part that is a measure of the reactive (or "near-field" or "source-generation") field.

Even for a simple, point source in linear acoustics, there is a reactive component of the acoustic intensity associated with the proximity of the source. We expect the secondary-frequency generation region to be a more complicated interaction region and hope that a measurement of both active and reactive intensity will reveal something of the nature of this region.

In the time domain, acoustic intensity is the time average of the product of acoustic pressure and particle velocity. In the frequency domain, the complex acoustic intensity is the product of the complex conjugate of the complex pressure and the complex particle velocity. One-half the real part of this product is identical to the time-domain time average and is a measure of the propagating acoustic power in power per unit area (W/m^2). One-half the imaginary part is a measure of the cyclic transfer of energy between kinetic and potential without propagation.

Intensity sensors have several configurations. Fundamentally, they can be grouped into two categories based on the way in which they measure acoustic particle velocity. An acoustically small, neutrally buoyant body immersed in the acoustic field moves with the same velocity as the local acoustic particle velocity. If that body holds a velocity sensor or an accelerometer, then the particle velocity can be measured directly. Often the body is not neutrally buoyant but this can be accounted by a correction factor. An intensity sensor based on this type of velocity measurement is an inertial intensity sensor. The inertial sensor used in this experiment measures pressure and particle acceleration (a *p-a* probe).

Since complex intensity is one-half the product of the complex conjugate of the complex pressure and the complex particle velocity, the intensity can be determined from the pressure-acceleration probe as follows:

$$I_{active} = \frac{1}{2}\mathrm{Re}\left[P^* V\right]; \qquad I_{reactive} = \frac{1}{2}\mathrm{Im}\left[P^* V\right] \tag{2}$$

where the complex particle velocity, V, is determined from the accelerometer output ($V = A/j\omega$).

Particle velocity can also be measured indirectly by measuring the acoustic pressure gradient. Two pressure sensors spaced a distance, d, apart in the x direction can be used to approximate the pressure gradient in the x direction by their difference,

$$V_x = \frac{j}{\omega\rho}\frac{dP}{dx} \approx \frac{j(P_2 - P_1)}{\rho c k d} \tag{3}$$

and the pressure by their average,

$$P \approx \frac{1}{2}(P_1 + P_2) \tag{4}$$

An intensity sensor based on this type of velocity inference is a pressure-differencing probe (or *p-p* probe). The intensity spectra can be determined from the two-hydrophone pair as follows:

$$I_{active} = \frac{1}{2\rho c k d}\mathrm{Im}\left[P_1^* P_2\right] = \frac{P_1^* P_1}{2\rho c k d}\mathrm{Im}\left[\frac{P_2}{P_1}\right] \tag{5}$$

$$I_{reactive} = \frac{1}{4\rho c k d}\left[P_1^* P_1 - P_2^* P_2\right] = \frac{P_1^* P_1}{4\rho c k d}\left[1 - \left|\frac{P_2}{P_1}\right|^2\right] \tag{6}$$

Normally, an inertial measurement is preferred because it involves direct measurement of velocity but inertial measurement is not practical in some cases. It is far easier to make a neutrally buoyant (or nearly neutrally buoyant) sensor in water than in air; however, it is more difficult to make inertial sensors small enough so that their housings are acoustically compact at very high frequency. Consequently, in air and for high frequency in water, the pressure-differencing probe is used more commonly. In the present measurement with a secondary frequency of 5 kHz in water, an inertial probe is practical. Both a *p-a* probe and a *p-p* probe were used in this investigation.

III. Test Configuration

The source for this series of measurements is a single panel from the four-panel NUWC TOPS projector. The projector is driven at 22 and 27 kHz so that a secondary at 5 kHz is produced in the water. The TOPS panel is shown on the left in Fig. 2. The radiating face is 17 inches wide by 21 inches tall. The two intensity sensors and their support cage are shown on the right.

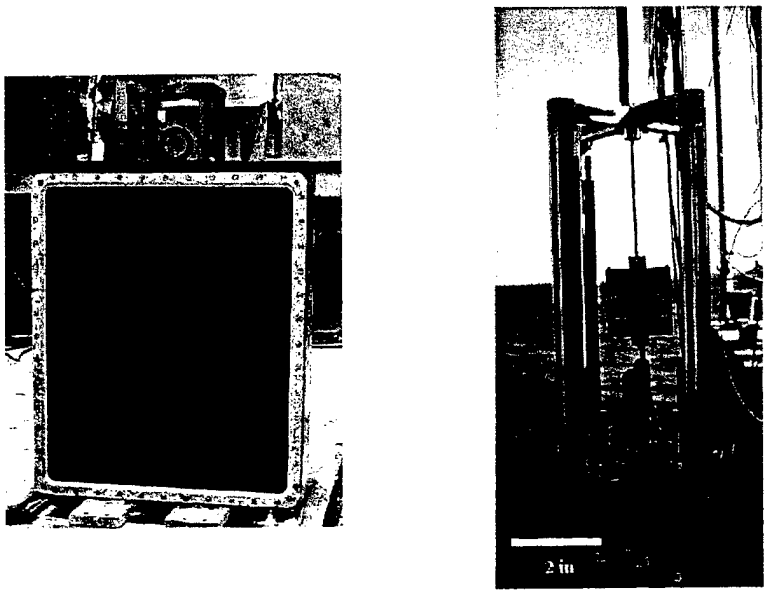

Figure 2. The TOwed Parametric Sonar (TOPS) projector panel on the left has a radiating face 21 inches by 17 inches and produces the primary beams at 22 kHz and 27 kHz simultaneously. The sensor assembly shown on the right measures acoustic intensity. At the center of the cage is the inertial acoustic intensity sensor (the *p-a* probe). Just below are the two pairs of hydrophones that make up the pressure differencing intensity sensor (the *p-p* probe).

The intensity measurements were made with two intensity sensors as sketched in Fig. 3. The first is a two-axis inertial sensor (the biaxial *p-a* probe – below left) that consists of a negatively buoyant body with two orthogonal accelerometers embedded inside. Part of the body is a piezoelectric cylinder hydrophone that provides the pressure measurement. The probe is 35 mm in diameter and 35 mm long with an overall density 2.8 times that of water. Because of the higher density, the amplitude of probe motion is 0.46 times that of the acoustic particle motion. If a is the radius of the probe cylinder, then ka at 5 kHz is 0.38 (and ka at 24.5 kHz is 1.8).

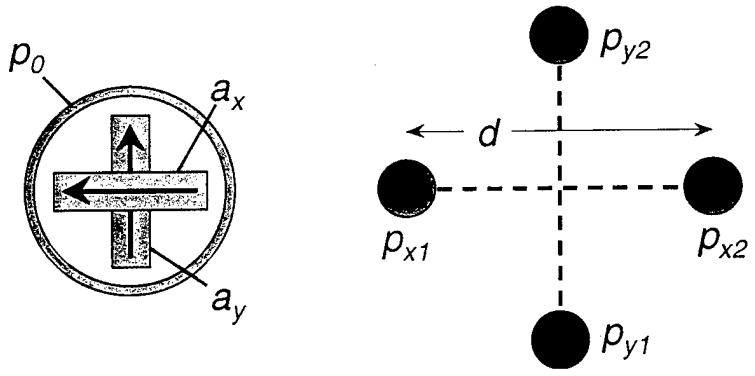

Figure 3. The two varieties of acoustic intensity sensors used in this experiment. On the left is a schematic of the inertial sensor (*p-a* probe). The *p-a* probe has two accelerometers embedded in a negatively buoyant body. The shell of the body is a piezoceramic cylinder that serves as the hydrophone and the accelerometers measure two orthogonal components of acoustic particle velocity. On the right is a schematic of the *p-p* probe. Each pair of hydrophones measures a component of particle velocity by determining the pressure gradient.

The second sensor is a two-axis pressure-difference probe (the biaxial *p-p* probe – above right) made from four omnidirectional hydrophones. The four hydrophones permit measurement of the gradient in two orthogonal directions (coincident with the axes of the inertial-sensor accelerometers). Opposing hydrophones are spaced d = 50 mm apart. At 5 kHz, kd is 1.1. Both intensity sensors were mounted on a common frame with their sense axes aligned.

Since intensity is a vector measurement, it is important to maintain alignment of the sensor with the projector. As indicated in Fig. 4, this was accomplished by rigging the sensor cage on a frame attached to two downrigger cables. The frame was clamped to one downrigger cable and fitted with a sliding attachment to the other cable. The other cable served to maintain alignment of the frame while still permitting adjustment of depth.

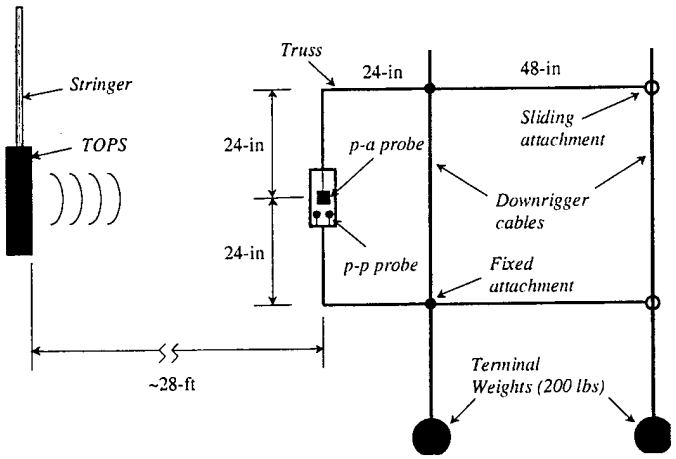

Figure 4. The configuration of the sensors and the source. The TOPS projector (on the left) was fixed at 30 meters depth but was rotated to sweep the beam through the sensors in azimuth. A frame attached to a downrigger cable to permit varying the depth supported the sensor cage (center). A second downrigger cable (right side) maintained the orientation of the frame so that the sense axes were always properly aligned with the source.

Perhaps the most important feature of a receiving sensor for this type of measurement is exceptional linearity. Since the efficiency of parametric generation is so low, the secondary pressure amplitude can easily be less than 0.01 times the amplitude of the primary (with acoustic intensity a factor of 10^4 lower). *One- percent distortion in the receiving sensor (at the primary frequency) would produce a false difference-frequency component as large as the parametrically generated component.* So the receiving sensor must have good linearity (< 0.1 % second-order distortion) at signal levels produced by the primary but still reproduce the received secondary signal 40 dB lower. Furthermore, measuring to 40 dB below the on-axis level of the secondary means that levels 80 dB below the on-axis primary level would be expected when measuring off axis.

IV. Characteristics of the Projector

The TOPS projector panel was submerged to a depth of 30 m and oriented with its long dimension vertical. At 24.5 kHz (the average of 22 and 27), the projector is about 9 wavelengths tall (0.53 m) and about 7 wavelengths wide (0.43 m) assuming a sound speed of 1450 m/s.

The TOPS projector was driven with 150 ms pulses. The pulses were digitally generated sums of 22 kHz and 27 kHz sine waves. The source level for the 22 kHz component was 229 dB (with respect to 1 μPa at 1 meter) and the source level for the 27 kHz component was 231 dB (same reference). The received level at 5 kHz (8.5 meters from the projector) was 168-170 dB with respect to 1 μPa.

Figure 5 shows the beam pattern for the primary beam in the horizontal plane. This beam pattern was generated for single-frequency excitation of TOPS at 25 kHz, but is representative of the pattern at either actual primary frequency. Also plotted on the same amplitude scale is the beam pattern for the secondary at 5 kHz (red) when the projector was driven with 22 and 27 kHz. The level of the secondary beam on the main axis is about 43 dB below that of the primary beam.

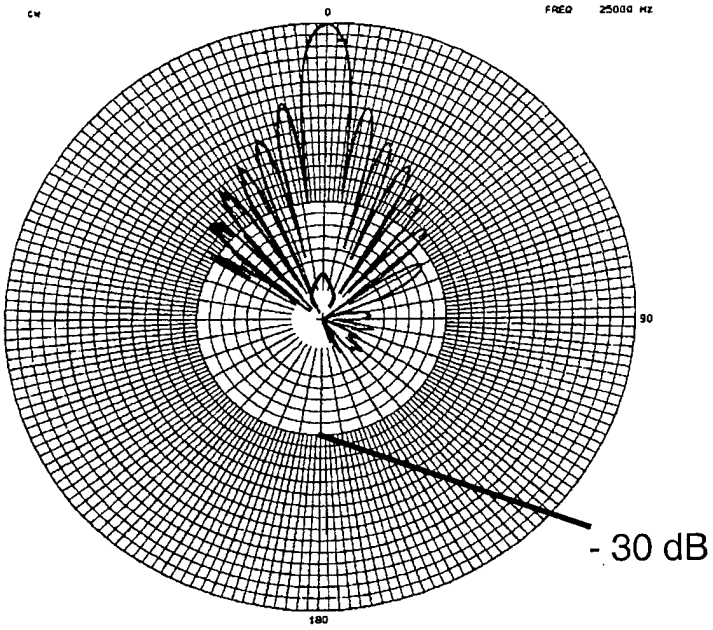

Figure 5. The primary and secondary beam patterns measured using a reference hydrophone 11 meters from the projector. The primary beam pattern (in azimuth) is shown as the black curve. This measurement was made at 25 kHz but is representative of either of the actual primary beams at 22 kHz and 27 kHz. The secondary beam pattern is shown in red on the same amplitude scale as the primary. This illustrates the substantial level difference between the primary and the secondary waves.

Often, the measured secondary pressure is reduced to an apparent source level. This is accomplished by multiplying the received pressure by the distance to the source transducer (equivalent to adding 20 log r – 18.6 dB at 8.5 m – to the pressure level in dB). While this is convenient when making crude performance estimates using a sonar-equation based model, it is misleading otherwise. The transducer does not generate the secondary; the secondary is produced in a continuous region of the *water* in the primary beam. The position of the transducer only serves to mark the start of the secondary source region. By translating the received pressure back to the transducer location, elements of the source region close to the hydrophone are dramatically overemphasized compared to elements of the source region close to the projector. Such a calculation results in a source level that is a function of range and does not represent the process of power generation in the beam accurately.

Figure 6 shows the beam pattern for the secondary beam normalized so that the on-axis level is 0 dB. This pattern shows much lower sidelobes than the primary beam, which is characteristic of parametrically generated beams. The 3-dB beamwidth is slightly smaller than the 3-dB beamwidth of the primary beam but the 20-dB beamwidth is broader than that of the primary. There are several sidelobes on the secondary beam pattern. Theoretically, the parametric beam should have no sidelobes; however, the radiation from the projector is not purely 22 and 27 kHz. As discussed below, nonlinearity in the power amplifier produces a drive component at 5 kHz. While the projector's transmitting response is considerably lower at 5 kHz than at 20 kHz, there is still a low level of direct radiation from the transducer at 5 kHz and this may be the cause of the sidelobes. Notice that the sidelobes have a much larger angular spacing than those in the primary pattern. This is consistent with direct 5 kHz radiation from the transducer. Notice also that the level of the lobes is about 40 dB below the peak, which is itself about 40 dB below the primary level at the receiver so the projector does not need to be very efficient at 5 kHz to produce observable radiation.

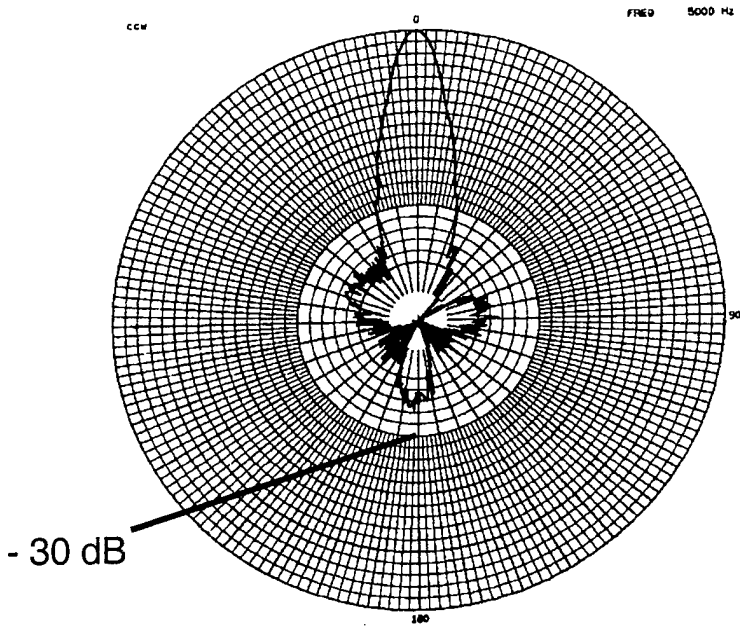

Figure 6. The secondary beam pattern from Fig. 5 normalized so that its maximum is 0 dB. The beam is somewhat wider than the primary beam but the sidelobes are much lower. Ideally, there would not be any measurable sidelobes for the secondary beam but, in this case, there may be some direct radiation from the projector at 5 kHz caused by nonlinearity in the projector drive amplifier.

The character of the primary beams can be estimated (roughly) by considering the projector to be a circular piston with an effective radius, a_{eff}, that gives the same surface area (so $a_{eff} = 0.27$ m). At 22 kHz, ka_{eff} is 26 and at 27 kHz, ka_{eff} is 32. For on-axis pressure, the location of the final interference peak occurs at $r = a_{eff}^2/\lambda$ or, at 24.5 kHz, $r = 1.2$ m. The Rayleigh length ($\pi a_{eff}^2/\lambda$) is about 4 m. Consequently, the primary beam is well collimated to slightly beyond one meter and has completed the transition to ordinary spherical spreading by about four or five meters.

V. Influence of Nonlinearity

There are at least three important sources of nonlinearity in this measurement:

(a) nonlinearity in the projector power amplifier,
(b) nonlinearity in the water, and,
(c) nonlinearity in the receiving sensor/electronics.

The second, nonlinearity in the water, is the desired effect but, because this effect is so weak, other sources of nonlinearity must be considered and eliminated or reduced.

The waveform for the projector is synthesized by a digital sum of two sine waves over a 150-millisecond time window. Even though the individual sine waves have some second harmonic, the digital summation is linear to the extent that the difference frequency is not measurable by the spectrum analyzer (see Fig. 7).

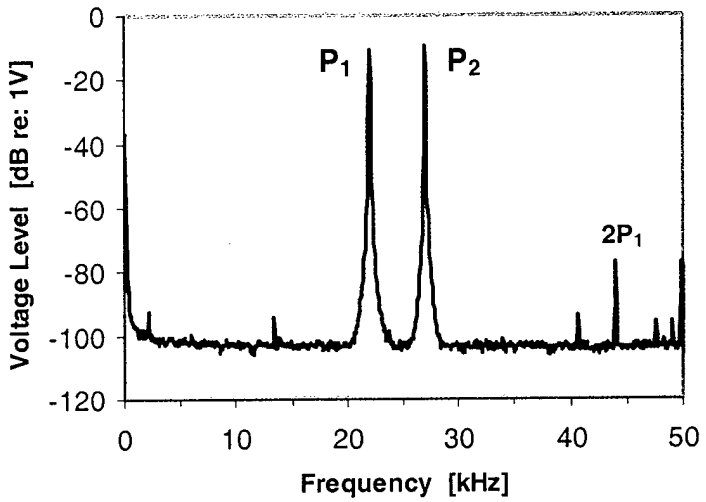

Figure 7. Spectrum of the synthesized waveform with the sum of the two primary-frequency signals (P_1 and P_2). While there is a measurable second harmonic of P_1 (and, presumably, P_2 beyond the right edge of the spectrum shown), there is no difference-frequency component.

Some parametric sources have two sets of transducer elements: one set is driven at one primary frequency and the other set is driven at the other primary frequency. In this way, nonlinearity in the drive amplifier or in the transducer itself does not produce a difference frequency component. However, all the elements of TOPS are driven with the same signal so the combination of the two primary sine waves is passed through the power amplifier and distortion in the power amplifier produces components at the difference frequency (and the sum frequency and other nonlinear combination frequencies). Since there is often a tradeoff between high efficiency and high linearity in power amplifiers, the drive signal for a high-power projector is likely to include a significant component at the difference frequency (see Fig. 8).

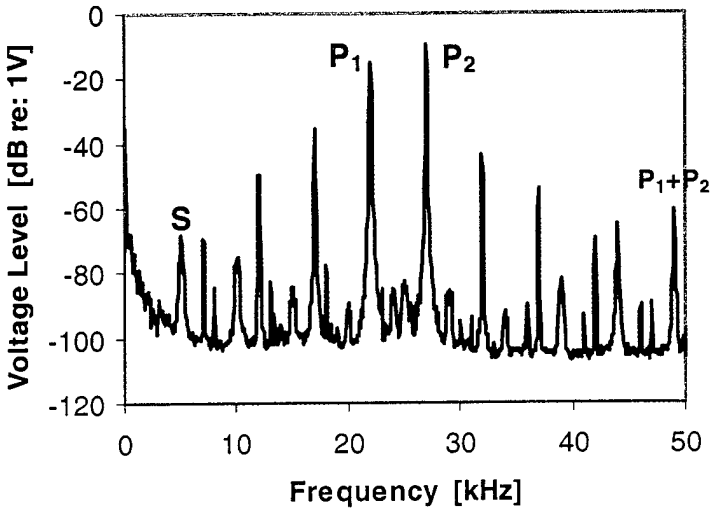

Figure 8. Spectrum of the voltage monitor signal at the output of the projector power amplifier. Here, nonlinearity in the power amplifier has produced a number of intermodulation products from the input (Fig. 7). There is a clear component now at the secondary (S) frequency. While this component is much smaller than the primary signals and the projector response is lower at 5 kHz than at 22 and 27 kHz, there may still be sufficient radiation at 5 kHz to be seen in, for example, the secondary beam pattern in Fig. 6.

The problem of direct radiation at the secondary frequency is usually mitigated by the response of the projector. The projector is designed for efficient transmission at the primary frequencies and the transmitting voltage response is normally considerably lower at the secondary frequency. However, at least in the early stages of evaluation of a parametric system, the projector should be intentionally driven directly at the difference frequency to examine the field produced.

For example, if the secondary frequency is produced directly by the projector, the beam pattern will reflect the projector size-to-wavelength ratio at that frequency; if the secondary is produced by nonlinear interaction in the water, then the beam pattern will reflect the primary beam characteristics. If most of the secondary power is produced by nonlinear interaction in the water, lower levels of direct radiation may be more obvious in the sidelobes at the secondary frequency (since the parametric beam should not have sidelobes).

For the TOPS array radiating directly at 5 kHz, there would be lobes at (about) +90, -90, and 180 degrees. Such a lobe structure is shown in the secondary beam pattern plot of Fig. 6. The sidelobe levels shown in the plot correspond to a direct-radiation component at 5 kHz about 70 dB below either primary component (or 25 dB below the parametric 5 kHz component at the receiver).

Figure 9 shows a spectrum that is representative of the received signal from TOPS operating as described earlier. Besides the primaries and the difference frequency, there are many other components in the spectrum. Some are generated by nonlinear interaction in the water but the projector radiates other components directly.

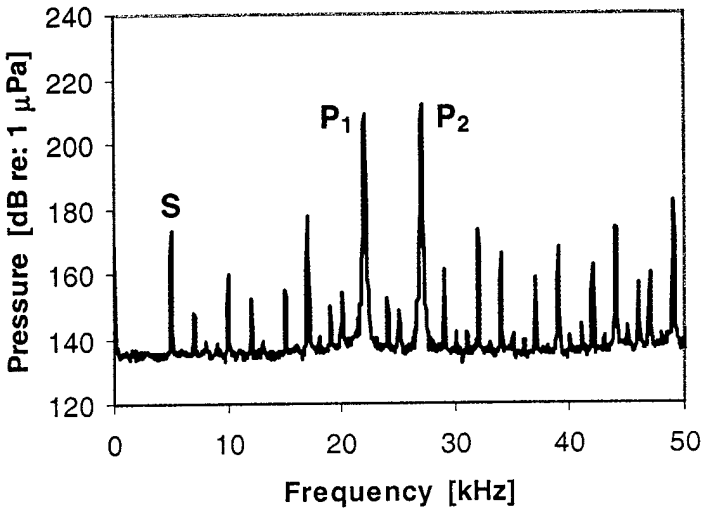

Figure 9. A typical received spectrum at 8.5 meters from the projector. There are many components beyond the two primaries and the secondary. Some are produced by direct radiation from the projector and some are generated by nonlinearity either in the water or in the receiving system. Note the similarity between this spectrum and the spectrum of the voltage monitor signal in Fig. 8.

It is more difficult to separate nonlinear generation in the receiving transducer from nonlinear interaction in the water because both phenomena reflect the distribution of power at the primary frequencies. If all of the nonlinearity were in the receiving transducer and its electronics, the apparent beam pattern at 5 kHz would have the shape of the product of the two primary beam patterns. While this pattern does have sidelobes (in contrast to the expected parametric beam pattern), the sidelobes are at much lower levels than in the primary patterns. Not only are these sidelobes proportional to the product of two values (each considerably lower than the on-axis values), but the primary-pattern sidelobes at one primary frequency do not coincide with the sidelobes at the other primary frequency. Consequently, the product yields even smaller sidelobes than the square of either primary beam pattern by itself.

Several steps were taken in order to minimize nonlinear generation in the receiving transducer and its electronics. Capacitive voltage dividers were incorporated prior to the first stage of amplification to ensure that the signal voltage on the input of the amplifier was always far below the power-supply rails. For these measurements, the input to the first-stage amplifier was never more than 50 millivolts at either of the primary frequencies. This is more than a factor of 100 below the power-supply limits for that amplifier. This meant that the secondary level was less than 500 microvolts on the beam axis and less than 5 microvolts at the 40-dB down points. Consequently, the first stage was a low-noise amplifier and synchronous averaging further reduced the noise floor. With synchronous averaging (triggered by the projector waveform), the signal-to-noise ratio was better than 30 dB even for measurements 30 dB below the on-axis secondary level. For the 12-Hz noise bandwidth used, this corresponds to a system voltage range of 140 dB with stringent linearity requirements on the lower 100 dB.

An alternate approach that is particularly useful when the secondary frequency is a small fraction of either primary is to add a passive low-pass filter to the input of the first-stage amplifier. This reduces the level of the primary signal before the amplifier. However, because the passive filter

is only a one- or two-pole filter, the filter introduces a significant phase change well below the filter's cutoff frequency. For simple pressure measurements, this is not important but phase is important for intensity measurement. As long as the phase shift is stable, though, its effects can be removed through calibration.

For two distinct input frequencies, a difference frequency is produced by second-order response (quadratic nonlinearity) but not by third-order response (cubic nonlinearity). If the nonlinearity in response is anti-symmetric around the zero point, then the quadratic term is zero. If the output voltage were plotted as a function of the input voltage for an ideal amplifier, the ideal curve would be a straight line through the origin – anti-symmetric.

In a real differential amplifier, as the signal increases toward the positive supply rail, the instantaneous gain drops and as the signal decreases toward the negative supply rail, the instantaneous gain also drops. The curve relating output voltage to input voltage would be a straight line in the vicinity of the origin but away from the origin to either side, the curve would bend toward the horizontal. If the amplifier was biased in the center of its range and its characteristics were symmetric, then the departure from linear response would be odd-order (primarily third-order). On the other hand, even if the amplifier characteristics were symmetric about the voltage center point, biasing away from that point would introduce second-order nonlinearity and difference-frequency production. Consequently, a high-quality operational amplifier was used and the impedances on the positive and negative inputs were balanced to maximize the operating symmetry of the amplifier. A discrete-transistor front-end is often used for very low self noise but it is much more difficult to achieve the required linearity with a single-transistor front end. In addition, strong feedback (low gain) was used to further improve the linearity.

VI. Errors in the Intensity Probes - Theory

There is substantial value in having two distinctly different intensity probes in the same sound field. This is especially true if their errors accumulate differently. It is instructive to consider the overall error in intensity introduced by magnitude and phase errors in the probe components and this is simplest if the acoustic field is assumed to be a pure, traveling wave.

A. The pressure-differencing (p-p) probe

Consider hydrophones 1 and 2 to be the two elements of one axis of a pressure-differencing intensity probe and the elements are separated by a distance, d, in the direction of propagation. Each hydrophone produces a signal that can be converted to equivalent pressure at the hydrophone and each hydrophone and electronics has its own error in magnitude and phase. The apparent pressures in the plane-wave field at each hydrophone are

$$P_1 = \alpha_1 P_0 e^{j(\omega t + \phi_1)} \; ; \qquad P_2 = \alpha_2 P_0 e^{j(\omega t + \phi_2 - kd)} \tag{7}$$

where α is the magnitude error of the hydrophone and its electronics and ϕ is the phase error. If these expressions are substituted into the equations for intensity,

$$I_{active} = \frac{P_0^2}{2\rho c} \frac{\alpha_1 \alpha_2 \sin(kd - \Delta\phi)}{kd} \tag{8}$$

and

$$I_{reactive} = \frac{P_0^2}{2\rho c} \frac{\alpha_1^2 - \alpha_2^2}{2kd} \tag{9}$$

where $\Delta\phi = \phi_2 - \phi_1$. Notice that the reactive intensity is unaffected by the relative phase mismatch, $\Delta\phi$, between the two hydrophones. Notice also that a small kd, which reduces the measurement error when the sensors are perfectly matched, increases the error in the magnitude of both components when there is some mismatch between the elements.

B. The inertial (p-a) probe

Consider a hydrophone and accelerometer 1 as the on-axis sensor pair of a *p-a* probe and the same hydrophone and accelerometer 2 as the cross-axis sensor pair. In a pure traveling wave field, the apparent pressure and velocities including sensor error are

$$P = \alpha_0 P_0 e^{j(\omega t + \phi_0)} \tag{10}$$

$$V_1 = \alpha_1 \cos\theta \frac{P_0}{\rho c} e^{j(\omega t + \phi_1)} \tag{11}$$

$$V_2 = \alpha_2 \cos\theta \frac{P_0}{\rho c} e^{j(\omega t + \phi_2)} \tag{12}$$

A sensor alignment error, θ, has been included also. Substituting these values into the expressions for intensity for the *p-a* probe yields,

$$I_{active} = \alpha_0 \alpha_1 \cos\theta \cos(\Delta\phi) \frac{P_0^2}{2\rho c} \tag{13}$$

$$I_{reactive} = \alpha_0 \alpha_1 \cos\theta \sin(\Delta\phi) \frac{P_0^2}{2\rho c} \tag{14}$$

$$I_{active-cross} = \alpha_0 \alpha_2 \sin\theta \cos(\Delta\phi) \frac{P_0^2}{2\rho c} \tag{15}$$

Equation (15) is for the active intensity in the cross-axis direction. The reactive intensity for the *p-a* probe is proportional to the sine of $\Delta\phi$ (or to $\Delta\phi$ for small $\Delta\phi$) whereas the active intensity for the *p-a* probe is proportional to the cosine of $\Delta\phi$ (or to one for small $\Delta\phi$). Consequently, in contrast to the *p-p* probe, the reactive intensity measurement by the *p-a* probe is sensitive to the relative phase error between the pressure sensor and the accelerometer, whereas the active intensity measurement is not. Neither of the on-axis quantities are very sensitive to the alignment error; however, the cross-axis intensity is.

VII. Summary of Measurements

The first measurement is a diagnostic assessment of the pressure hydrophones. Nonlinearity in the receiving sensor and electronics is indicated (at least in some instances) by a narrow peak superimposed on the beam pattern measurement. The narrow peak appears on the beam axis riding on top of the broader peak of the true secondary beam.

Figure 10 compares the beam pattern determined from each of the four hydrophones in the *p-p* probe assembly with a reference hydrophone at a longer range. There is no obvious protrusion in any of the five patterns on the beam axis. The rotation fixture holding the TOPS projector was not zeroed at the main beam axis so the axis appears to be at –8 degrees. This is not 8 degrees with respect to the perpendicular to the TOPS array; the zero point in the azimuth plots has no special significance (but the angular scale is consistent from plot to plot).

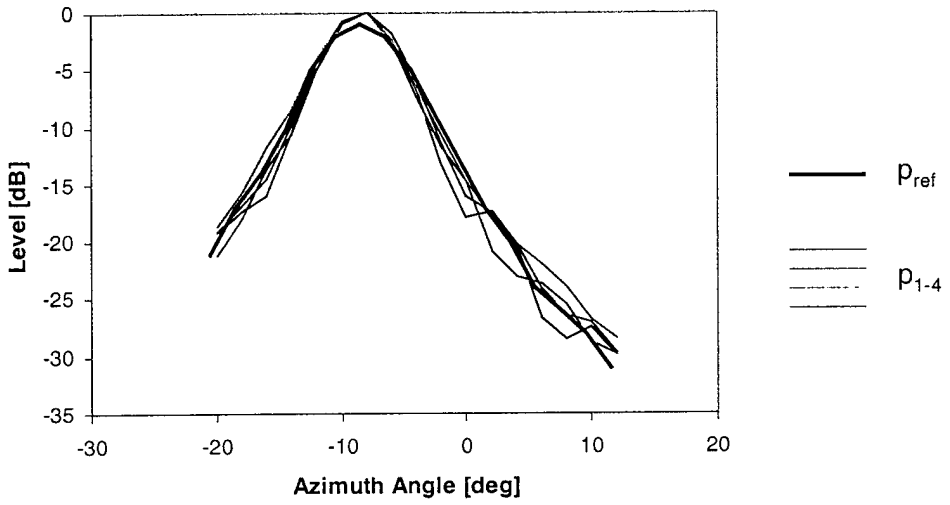

Figure 10. Beam patterns (in azimuth) as measured by a reference hydrophone (p_{ref}) and by the four hydrophones (p_{1-4}) that comprise the *p-p* probe.

Figure 11 shows the acoustic intensity at 5 kHz as a function of azimuth angle (polar plot) as measured by the *p-a* probe. Rotating the TOPS projector changed the angle. The radial scale reflects the intensity (in dB) with respect to the intensity that would result from a plane wave with an rms amplitude of 1 μPa. In other words, if the wave field were that of a pure traveling wave, the value indicated would also equal the sound pressure (in dB with respect to 1 μPa) indicated by a hydrophone. This value can be converted to dB with respect to 1 W/m^2 by subtracting 182.

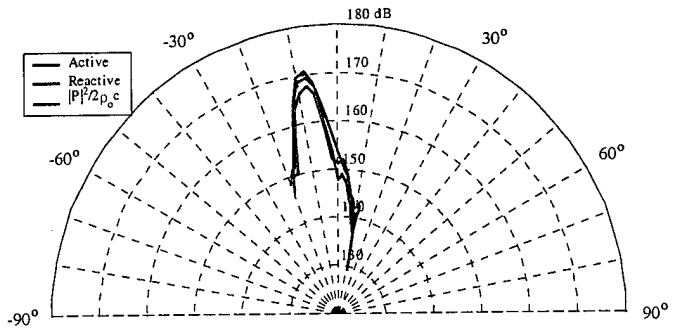

Figure 11. Active (blue) and reactive (red) acoustic intensity as measured by the on-axis component of the *p-a* probe. The green curve is the active intensity that would be observed if the wave were a pure traveling wave.

The blue curve in Fig. 11 is the active intensity measurement; the red curve is the reactive intensity measurement; and the green curve is the ordinary pressure measurement. In this figure, the intensity was measured using the on-axis accelerometer and pressure sensor. The measurement indicates an active intensity comparable to the ordinary pressure measurement and a somewhat lower reactive intensity. This suggests a field with a strong traveling wave component and a weaker but substantial reactive or source component; however, the discussion below will cast some doubt on the validity of the reactive intensity measurement.

Figure 12 shows similar results for the *p-a* probe using the cross-axis accelerometer. These measurements should indicate the intensity perpendicular to the main beam. Both the active and the reactive intensity values are considerably lower than for the on-axis measurement. The actual values are probably even lower: the measurement is a vector measurement and, if there were a small angular misalignment in the probe, the "cross-axis" measurement would be influenced by the projection of the on-axis intensity vector onto the misaligned sensor. An alignment error of only three degrees would be sufficient to account for the levels shown here even if the actual cross-axis intensity were zero. In fact, the cross-axis measurement may be used to align the apparatus. By symmetry, the active intensity perpendicular to the beam should be zero on the main axis (there being no preferred direction for propagation perpendicular to the beam) and the probe could be aligned by rotating to null the cross-axis active intensity.

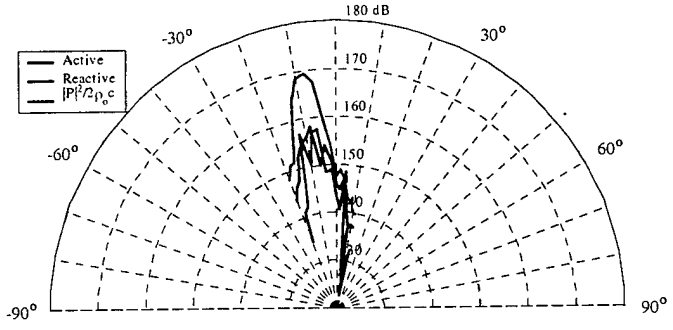

Figure 12. Active (blue) and reactive (red) acoustic intensity as measured by the cross-axis component of the *p-a* probe. The green curve is repeated from Fig. 11 for reference.

Figure 13 combines results from the *p-p* probe and from the *p-a* probe for active intensity. The red curves are for on-axis intensity and the blue curves are for cross-axis intensity. The *p-a*

probe results are plotted as the thick curves and the *p-p* probe results as the thin curves. Except for the region within four degrees of the main-beam axis, the results for on-axis active intensity agree well between the *p-a* probe and the *p-p* probe.

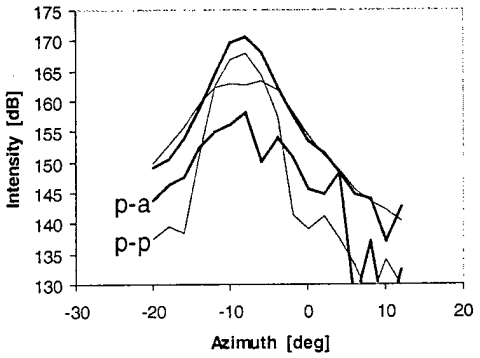

Figure 13. A comparison of the active intensity calculated from both the *p-a* probe and the *p-p* probe. The red curves are active intensity in the on-axis direction and the blue curves are active intensity in the cross-axis direction. The thicker curves are for the *p-a* probe. Notice that the on-axis intensity values between the two probes compare well except for a region within four degrees of the peak.

The on-axis active intensity as determined from the *p-a* measurements follows the secondary beam pattern closely. Near the beam axis, the *p-p* measurement does not. As discussed in the section on intensity-probe errors, relative phase errors in the *p-a* probe have little influence on active intensity whereas the active intensity determined by the *p-p* probe *is* sensitive to relative phase errors. Notice also that the agreement between the *p-a* probe and *p-p* probe with respect to cross-axis active intensity is poor.

Figure 14 shows the measured phase difference between pairs of hydrophones in the *p-p* array. The cross-axis pair (blue curve) should show a nearly zero phase difference if the wavefront is plane and perpendicular to the beam axis. Except for the region within four degrees of the main axis, this is roughly true. The on-axis pair (red curve) should show a phase difference equal to the wave number at 5 kHz times the separation. There is more scatter in the on-axis phase difference but outside the region within four degrees of the main beam axis, the phase oscillates around the expected 70 degree difference.

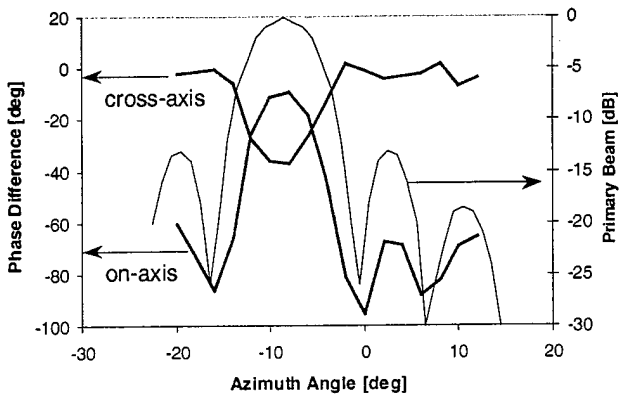

Figure 14. Measured phase difference between hydrophones in the *p-p* probe as a function of azimuth angle. The red curve is the phase difference between the on-axis pair and the blue curve is the phase difference between the cross-axis pair. Except for the region within four degrees of the peak, the phase differences correspond to the expected phase difference in each case. The primary beam pattern is plotted in black (with the amplitude scale on the right side). Notice the correlation between features in the phase differences and features in the primary beam pattern.

For reference, the beam pattern of the primary beam is plotted as the thin black curve (with the amplitude scale on the right side of the plot). Notice that the greatest departure of the phase difference from the expected phase difference occurs for the highest primary level. Notice that the pattern of the cross-axis phase difference nearly matches the pattern of the primary beam.

This correlation between phase difference and primary level could be interpreted in at least two ways. One interpretation is that the generation of the secondary is strongest when the primary levels are highest so the reactive contribution would also be highest here. The greatest departure from simple traveling wave behavior would occur near the peaks in the primary pattern. Another interpretation is that the high primary levels corrupt the measurement. This would also produce a match in shape between the phase difference and the primary pattern.

This issue cannot be entirely resolved without further measurements but there are several suggestive clues in the present measurements. If the apparent departure from a pure traveling wave field is real and both the *p-a* and the *p-p* probes are recording the field accurately, then their assessments of the field would be very similar. This is clearly not the case. The on-axis active intensity determined from the *p-p* probe results is substantially different than that determined from the *p-a* probe results in the vicinity of the beam axis. (And the same is true for the on-axis reactive intensity.)

Since the active intensity from the *p-a* probe matches the ordinary secondary beam pattern so well, it is tempting to conclude that the *p-a* results are correct and the *p-p* results are flawed. This may be true, however, it is worth examining the results more closely. From the discussion of probe error above, inter-element phase errors (whether hydrophone-to-hydrophone or hydrophone-to-accelerometer) have a large effect on the active intensity calculation from the *p-p* probe but only a small effect on the active intensity calculation from the *p-a* probe. Consequently, an equally plausible supposition is that the inter-element phase is not being measured correctly on both probes.

As a partial test of this supposition, the intensity from the *p-p* probe was recalculated using the average inter-element phase difference over azimuth (but excluding the region within 4 degrees of the main axis from the average). These results are shown in the Fig. 15. The correspondence between the *p-a* probe and the *p-p* probe for on-axis active intensity is excellent and the agreement for cross-axis active intensity has improved substantially.

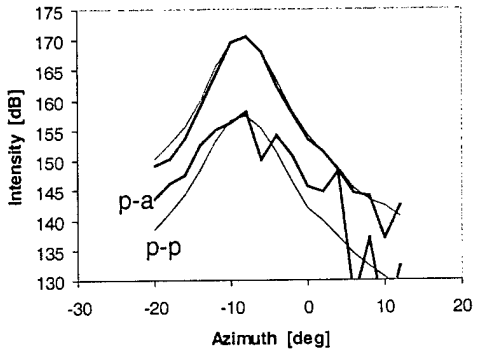

Figure 15. Active intensity for both the *p-a* probe and the *p-p* probe. The results from the *p-p* probe have been recalculated based on the average phase difference excluding the window within four degrees of the peak. The results from both probes agree well with this correction but the justification for such a correction is weak.

It would be difficult to explain a significant cross-axis active intensity component on the beam axis but the cross-axis intensity shown in the figure is probably not an accurate measure of the intensity perpendicular to the beam direction. As discussed above, a pointing error of only three degrees would be sufficient to produce the results shown in the figure even if the cross-axis intensity were zero. Away from the beam axis, there could be a small active intensity component perpendicular to the beam but the component should be symmetric about the beam axis – zero at the center and away from the beam axis on *both* sides.

At this point, it is tempting to conclude that the *p-a* probe is accurate and the *p-p* probe is not but we need to examine the reactive intensity as well. The situation with regard to inter-element phase error is reversed for reactive intensity. The reactive intensity calculation for the *p-p* probe does not involve phase at all, whereas the reactive intensity calculation for the *p-a* probe is sensitive to inter-element phase error. The results for on-axis reactive intensity are shown in Fig. 16. The red curve is the on-axis *active* intensity from the *p-a* probe for reference. The thick blue curve is the reactive intensity determined from the *p-a* probe and the thin blue curve is the reactive intensity determined from the *p-p* probe. If phase errors were the only errors in the measurement, then the *p-p* result would be accurate. The reactive intensity from the *p-p* probe is lower than that from the *p-a* probe and more consistent with the understanding that the field at 8.5 meters would be predominantly traveling wave (since the strongest region of interaction is at shorter ranges) with a smaller source-generation component.

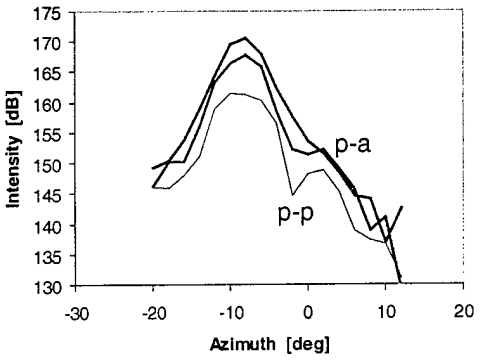

Figure 16. The on-axis reactive intensity. Here, the on-axis active intensity is plotted in red for reference. The blue curves are reactive intensity with the thicker curve from the *p-a* probe.

Since, however, both of the reactive intensity curves mirror the shape of the primary beam, we are still left with an ambiguous interpretation. The *p-p* reactive intensity calculation could be correct (and the *p-a* calculation corrupted by inter-element phase error) or both calculations could be corrupted by error. While the *p-p* reactive intensity calculation is completely insensitive to phase errors, it is sensitive to inter-element magnitude errors.

The most conservative interpretation of these measurements is that the on-axis active intensity has been determined with reasonable accuracy through the secondary beam and that all of the determinations of reactive intensity are suspect. A more speculative interpretation is that the *p-p* probe determination of on-axis reactive intensity is representative of the source-generation mechanism but may be corrupted to some degree by the presence of the high-level primary beams. These problems in interpretation probably cannot be resolved entirely from the present measurements; however, they probably can be understood with diagnostic experiments in the lab.

VIII. Errors in the Intensity Probes – Measurement and Calibration

So far we have not tried to identify the source of any inter-element phase (or magnitude) errors. There are at least two possibilities. The obvious source is in calibration error of the individual elements. A less obvious source is a phase error produced by scattering of the field by the sensor structure. While the scattering is expected to be weak at 5 kHz, the scattering would be strong at 22 kHz and 27 kHz.

In normal underwater use, inertial intensity sensors outperform pressure-differencing intensity sensors because the inertial sensors measure particle velocity directly while the differencing sensors infer the particle velocity from a finite-difference approximation to the pressure gradient. There is, however, one advantage that the *p-p* probe has in practice although this advantage is rarely exploited. The relative response of the two elements of a *p-p* probe can be determined very accurately by means of interchange calibration. If two pressure sensors are placed in an arbitrary acoustic field, the ratio of their outputs (magnitude ratio and relative phase) can be measured:

$$e_{A1} = M_A P_1 \; ; \quad e_{B1} = M_B P_2 \; ; \quad \frac{e_{B1}}{e_{A1}} = \frac{M_B P_2}{M_A P_1} \tag{16}$$

Here, sensor A (with response M_A) is at a position where the acoustic pressure is p_1 and sensor B (with response M_B) is at a position where the acoustic pressure is p_2. All quantities are complex and the sensor outputs (including all amplification, cables, analyzer input electronics) are given as the voltages, e_{A1} and e_{B1}.

If the two sensors are interchanged with regard to position in the field, the ratio of their outputs can again be measured:

$$e_{A2} = M_A P_2 \; ; \quad e_{B2} = M_B P_1 \; ; \quad \frac{e_{B2}}{e_{A2}} = \frac{M_B P_1}{M_A P_2} \tag{17}$$

The complex square root of the product of the ratios gives the relative magnitude and phase response between the two sensors,

$$\sqrt{\frac{e_{B1}}{e_{A1}}\frac{e_{B2}}{e_{A2}}} = \frac{M_B}{M_A} = \left|\frac{M_B}{M_A}\right| e^{j(\phi_B - \phi_A)} \tag{18}$$

and the complex square root of the quotient of the ratios gives the complex ratio of the two pressures,

$$\sqrt{\frac{e_{B1}/e_{A1}}{e_{B2}/e_{A2}}} = \frac{P_2}{P_1} \tag{19}$$

Since the intensity results are far more sensitive to relative errors than to the absolute response of either hydrophone, the absolute response of one hydrophone is determined by a standard comparison calibration with a reference hydrophone (to within one or two dB). Then the relative magnitude and sensor/electronics phase difference is determined by interchange (to within a fraction of a degree and one or two *tenths* of a dB).

The interchange method does not require that the pressures be identical at each hydrophone, which means that the *p-p* probe can be rotated around its axis by 180 degrees from any starting point to perform the interchange. Since the starting position does not matter, a complete rotation of the probe with stops every 5 degrees (for example) yields 36 different sets of 180-degree interchanges. This permits averaging a number of measurements. A rotational interchange measurement every one degree (Fig. 17) was made in a calibration tank at the Applied Research Laboratory with the *p-p* probe. For the on-axis pair at 5 kHz, the ratio of magnitudes was 1.01 ± 0.01 (or 0.09 ± 0.09 dB) and the phase difference was 2.9 ± 0.2 degrees.

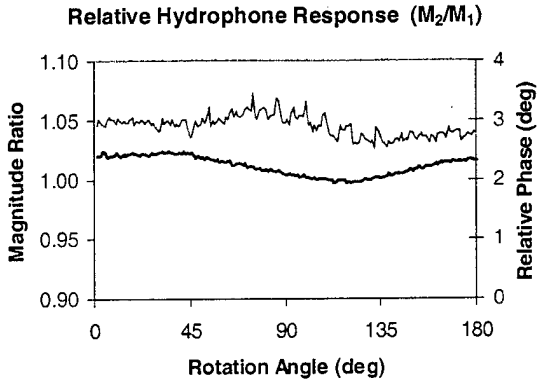

Figure 17. Results from a rotational interchange calibration at 5 kHz of the on-axis hydrophone pair in the *p-p* probe. The blue curve is the ratio of the amplitude response magnitudes and the red curve is the phase difference between the two hydrophones. The amplitude responses are within 0.1 dB and the phase difference is about three degrees within a few tenths of a degree.

The hydrophones in the *p-p* probe are sufficiently well matched that correction for the phase and magnitude mismatch determined by interchange makes only very minor changes in the intensity results. The rotational interchange measurement also produces the ratio of the acoustic pressure between the two sensors. This is shown in Fig. 18. A rotation angle of zero corresponds to an orientation in which the two hydrophones are in line with the source; a rotation angle of 90 degrees indicates that the hydrophone pair is oriented perpendicular to the direction of propagation.

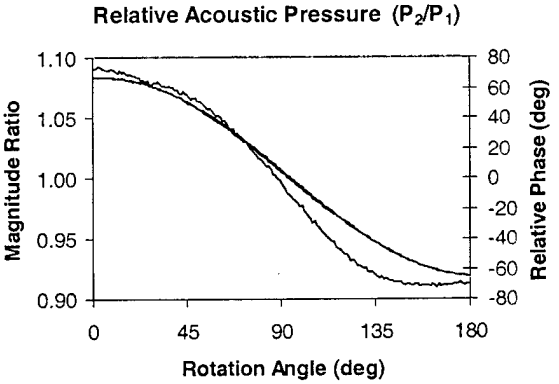

Figure 18. The interchange calibration at 5 kHz also produces a measure of the relative acoustic field between the two hydrophones. The magnitude ratio of the two pressures (blue) and their phase difference (red) are plotted here. As the pair is rotated, the phase should change from the spatial phase of the traveling wave over the hydrophone spacing at 0 and 180 degrees to zero when the pair is rotated perpendicular to the direction of wave propagation (90 degrees). The magnitude ratio should reflect only the difference in spreading between the two hydrophone positions (since p_2 is closer to the source by two inches than p_1 at the zero-degree position). The ratio is considerably higher indicating some scattering of the 5 kHz field by the sensor assembly.

The figure shows that the pressure at the hydrophone toward the source is about 1.09 times larger than the pressure at the hydrophone away from the source and the relative phase is about 65 degrees. The phase is consistent with the traveling wave but the amplitude ratio is significantly greater than the ratio of 1.02 from spherical spreading over the 2-inch separation at 3 meters

from the source. This suggests that scattering from the sensor assembly is not negligible even at 5 kHz.

Since the reactive intensity calculated from the *p-p* probe depends on the amplitude difference between the two hydrophones, scattering by the sensor assembly would produce an erroneous reactive level. Using the same amplitude difference determined by the rotational interchange measurement, the false reactive intensity would be about 20 dB below the active intensity. The reactive intensity from the *p-p* probe is (on the beam axis) only 10 dB below the active intensity so scattering at 5 kHz is not sufficient to explain the reactive measurement. Also, if scattering at 5 kHz produced the entire observed reactive field, the shape of the reactive intensity with respect to azimuth angle would not be similar to the primary beam pattern.

It is not clear how to apply interchange to the *p-a* probe, however. The relative response between the two orthogonal accelerometers can be determined by measurement in one orientation and measurement after a 90-degree rotation but the important comparison is between the response of the hydrophone and the on-axis accelerometer. These sensor elements were calibrated individually by comparison with a reference hydrophone and by assuming that the field in the calibration was that of a traveling wave (using short pulses at 5 kHz). Consequently, the relative magnitude and phase differences between the pressure sensor and the on-axis accelerometer are not determined with as much precision as in the *p-p* probe. Nevertheless, the response differences are much smaller to explain the observed anomalies in the intensity.

The discrepancy between the *p-a* probe and the *p-p* probe cannot be explained by inter-element response mismatch. In fact, it makes very little difference in the results whether the calibration corrections are applied or perfect matching is assumed. The discrepancy must have a different origin. Furthermore, any explanation of the discrepancy must account for the fact that the discrepancy is, in some cases, large. For example, if the *p-p* probe is producing erroneous values for the on-axis active intensity (and that seems to be the case), *a 60-degree phase correction* is required at the peak in the beam pattern to bring those results into line with those from the *p-a* probe.

Another possible source for error in the measurement is in nonlinear effects associated with the receiving sensor. We have taken many steps to minimize nonlinearity in the receiving system but it is still possible that sufficient nonlinearity remains to corrupt the results. The simple test for nonlinearity in the receiving system – the appearance of a narrow projection riding on top of the secondary beam pattern – may be misleading. For a measurement made well beyond the interaction region, the secondary pattern is determined by the length (and width) of the interaction region, not by the shape of the primary pattern at the receiver. Consequently, the secondary pattern could be considerably more broad than the primary pattern. Nonlinearity in the receiver would produce a false pattern similar to the primary pattern squared, which would appear as a narrow projection superimposed on the true secondary beam pattern. However, in or near the region of strong interaction, the shape of the primary pattern determines the shape of the secondary beam pattern. In this case, there would be much less difference (it seems) between the true secondary beam pattern and primary pattern squared (the false pattern resulting from nonlinear generation in the receiver).

If the discrepancy were caused by nonlinearity associated with the receiving sensor system, the errors would depend on the local amplitude of the primary field and that seems to be true.

Ideally, the local amplitude at any sense element is determined by the primary beam patterns. However, the sensor cage containing both the *p-a* probe and the *p-p* probe presents an acoustically large and complicated scattering body to the fields at 22 and 27 kHz. So the local amplitude at any sensor element may be considerably different than expected for ordinary plane waves at 22 and 27 kHz.

Any explanation for the probe results must account not only for the magnitude of the discrepancies between the two but also for the complexity of the results. One way to support or refute direct nonlinear generation from the incident primary waves is to measure carefully the response of the *p-p* (and *p-a*) probe to fields at the primary frequencies. Rotating the cage and monitoring the pressures at the various elements can assess the effects of the probe assembly on the incident field. An even better test would consist of transmitting high levels of 22 and 27 kHz using two different projectors with sufficient angular separation so that the primary beams only overlapped in the immediate vicinity of the probes. This way, there would be very little secondary generation in the water.

IX. Improvements and Lessons Learned

Since this experiment is the first measurement of acoustic intensity in the interaction region of a parametric source, the yield in lessons learned is greater than the yield in raw data. Many of the issues listed below are discussed in more detail in the body of this report; however, it is useful to compile the important results here.

1. The importance of linearity in the sensor and sensor electronics cannot be overemphasized. Parametric generation is inefficient so measurements of the secondary field are invariably performed in the presence of much higher levels of the primary fields. In many acoustic measurements, a system with one-percent second harmonic distortion would be considered highly linear. For the present measurements, one-percent distortion is far too high. The false secondary signal produced in the receiving sensor system would be larger than the true secondary signal.

2. The hydrophone amplifier should be designed carefully. A low-noise operational amplifier with balanced input impedances can be used as long as the input level is kept well below the input voltage limits. In the design process, the higher levels at the primary frequencies must be considered even if the secondary is the signal to be measured. Filtering prior to the first stage of amplification can improve the performance but the phase shift introduced by the filter must be considered if intensity is to be determined.

3. Minimizing nonlinearity in the sensor itself means ensuring that the internal strains in the piezoelectric material are very small for the expected primary field levels. The piezoelectric response is not linear for high amplitudes and there is a small but fundamental second-order response common to all dielectrics. For the hydrophones used, the primary acoustic pressure levels would have produced strains between 10 and 100 parts per million. While it is not clear that these levels of strain would produce significant nonlinearity, this effect should not be dismissed without further consideration.

4. In these measurements, a small voltage response to acoustic pressure is preferable to a large voltage response. This is suggested not only by the desire to maintain small internal stress but also by the need to keep the maximum voltage well below the first-stage amplifier limits. A solid, hydrostatic-mode element may be the most suitable hydrophone. In this experiment, the hydrophone response was roughly –240 dB (re: 1 μPa) and this was achieved with a capacitive voltage divider and a conventional air-backed cylinder hydrophone. It would have been better to use an element with a lower intrinsic response and dispense with the capacitive divider.

5. Physically large (comparable to a wavelength at either primary frequency) hydrophones should be avoided. Such hydrophones when placed in the field can cause local primary-frequency pressure increases and scattering of the primary field. While interactions of the scattered components are not expected to change the secondary field (since the interaction distances for the scattered components would be so small), increased acoustic pressure of the primaries on the hydrophone face would aggravate nonlinear generation in the hydrophone or its electronics.

6. Although it is common practice to calibrate the projector only at the primary frequencies, it is important to understand the projector's radiating characteristics at the secondary frequency. Unless the projector is split into two sets of elements and each set is driven by a separate primary waveform, nonlinearity in the drive amplifier will produce a low level of drive directly at the secondary frequency. By measuring the characteristics (transmitting voltage response and beam pattern) with direct drive at the secondary frequency, these effects can be separated from the phenomena caused by nonlinear interaction in the water.

7. In addition, the receiving characteristics of the hydrophone (or intensity sensor) should be measured at the primary frequencies. Lower levels at the primary frequencies can be used to understand scattering by the probe assembly. An even more useful test of the receiving sensor can be performed with two source transducers. If two source transducers separated in space and aimed toward the hydrophone so that their beams only overlap in the small region surrounding the hydrophone, then nonlinear interaction in the water can be minimized. By placing the source transducers close to the hydrophone, it may even be possible to duplicate the actual primary levels without extremely high-power transducers. In this way, the nonlinearity introduced by the hydrophone and its electronics can be determined quantitatively.

8. While the inertial intensity sensor (the *p-a* probe, in this experiment) is generally easier to use for underwater measurements than sensors of the pressure-differencing type, using both types in this series of measurements was of considerable value. With only one sensor, it is easier to miss problems and it is more tempting to put too much faith in the results. For some measurements, the two varieties of sensors used here did not agree. This leads to greater scrutiny and, ultimately, to greater understanding when the problems are resolved.

9. The *p-p* probe is a valuable tool for underwater intensity measurement if it is used carefully. Since *p-p*-based measurements are sensitive to element mismatch, the ability to perform the interchange calibration (even *in situ* with some modifications to the apparatus) largely removes this objection to the *p-p* probe. Also, the *p-p* results are more sensitive to mismatch between elements than to absolute calibration errors. Consequently, the spacing between the

hydrophones in the *p-p* pair can be made large to reduce substantially the effects of mismatch errors at the cost of a moderate increase in finite-difference error. The error equations for the *p-p* probe can be used to pick a reasonable spacing.

10. Synchronous averaging was used to advantage in these measurements because such a large overall system dynamic range was required. In synchronous averaging, the signal acquisition is triggered by the source waveform (with a delay appropriate to the propagation time). The received and sampled time waveforms are averaged before spectral analysis. The synchronization means that the desired signals are coincident in each waveform but the noise is not. Consequently, the signal-to-noise ratio is improved. (Ordinary rms averaging does not change the signal-to-noise ratio in the received signal; rms averaging only reduces the scatter in the spectral values.) For this process to work, it is essential that the source waveshape be identical for each transmission. With digital function synthesis, this is straightforward. The process is not useful if the transmitted waveform is a gated sine wave where the gated period may fall anywhere with respect to the sine wave cycle.

11. Because there is evidence of scattering by the sensor assembly even at the secondary frequency, the sensor assembly should be redesigned to increase the separation between the *p-a* probe and the *p-p* probe and between the probes and the cage elements.

12. Finally, parametric generation is also possible in air with relatively inexpensive transducers. While it is not practical to use a *p-a* probe in air, the *p-p* probe with *in situ* interchange should be capable of producing accurate measurements of acoustic intensity. Such measurements can be made in a dry laboratory setting at much lower cost than underwater and little scheduling or resource conflict problems. Further analysis of the interaction region in a parametric beam could be performed at low cost with substantial payback through a set of in-air experiments. The quality of subsequent underwater measurements would be enhanced by application of the techniques developed for the in-air experiments.

ACKNOWLEDGEMENTS

This work was supported by ONR Code 321SS (J. McEachern and K. Dial) under BOA N00014-00-G-0058/0024. The authors thank William Konrad and William Clay for providing TOPS and supporting apparatus and for their participation in the Lake Seneca test.